NANO LETTERS

Letter

pubs.acs.org/NanoLett

Plasmonic Properties of Metallic Nanoparticles: The Effects of Size Quantization

Emily Townsend* and Garnett W. Bryant*

Joint Quantum Institute and Quantum Measurement Division, National Institute of Standards and Technology, Gaithersburg, Maryland 20899-8423, United States

Supporting Information

ABSTRACT: We examine the size quantization of plasmons in metallic nanoparticles using time-dependent density functional theory. For small particles in the quantum limit, we identify "quantum core plasmons" and "classical surface plasmons", both of which are collective oscillations comprised of multiple single-particle transitions. As particle size increases, the response of the classical surface plasmons becomes much larger than that of the quantum core plasmons.

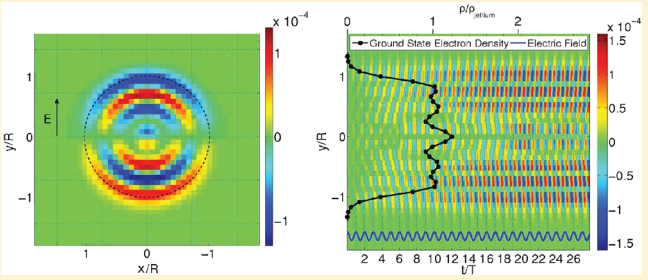

KEYWORDS: *Metallic nanoparticles, quantum plasmonics, surface plasmons, quantum core plasmons, size quantization, TDDFT*

Metallic nanoparticle (MNP) ensembles can guide and focus light on the nanoscale and alter the absorption or emission of light in a nearby optically active element. This opens the possibility of using MNPs in the transfer of quantum information. For example, arrays of MNPs can provide nanoscale control of optical signals, transferring light from one MNP to the next. To use that capability for control of quantum information, hybrid systems of nanostructures would need to absorb photons carrying quantum information, coherently transport that information and re-emit photon qubits, preserving entanglement. An accurate description of these processes requires an understanding of field confinement and enhancement due to plasmon resonances in the MNP, as well as the quantum hybridization between states of an absorber/emitter and of the MNP system. In this context, it is our goal to have a quantum description of an entire nanosystem, which may include multiple MNPs, metallic nanorods, semiconducting quantum dots, and other elements. Previous descriptions of such nanohybrid systems include those which use a classical description of the MNP via a frequency-dependent dielectric constant,[1−3] and models that begin with plasmons as quantum excitations whose properties are assumed or derived.[4−6]

The quantum description of plamons in MNPs began with Crowell and Ritchie,[7] who quantized a classical hydrodynamic model of an electron gas sphere. That class of approaches assumes from the outset the presence of plasmons as noninteracting modes, coupled to a radiation field. This was then extended to nanohybrid systems with MNP plasmons coupled to the radiation field as well as excitations of a dipole emitter[6] and to a dipole and the identical plasmon modes of a second MNP.[4]

The other quantum approach uses time-dependent density functional theory (TDDFT) to build a quantum description of MNPs from electron states rather than plasmons. In this work, we apply real-time, real-space TDDFT to a three-dimensional jellium model for metallic nanoparticles. The jellium model replaces the atomic potentials felt by electrons in a metal with that of a uniform positive charge density. This approximation is commonly used because it captures the most universal aspects of metallic nanoparticles, particularly the collective modes of the electronic motion.

Real-time and real-space TDDFT allows us to follow the dynamics of a variety of quantities under the influence of a time-varying potential, revealing the character of resonances with greater clarity. In addition to the optical spectrum of a MNP, we can see in detail where in the particle oscillations are occurring, how those oscillations are built up from changes in individual Kohn−Sham states and how selection rules govern those changes. We use this information to characterize the size quantization of MNP plasmons.

Early applications of TDDFT to a jellium sphere model were made by Ekardt,[8] Puska et al.,[9] and Beck,[10] using a frequency-space linear response formalism (sphere sizes up to 198 electrons (1.2 nm),[8] 92 electrons (0.78 nm),[9] and 198 electrons (0.62 nm),[10] respectively). These authors calculated photo-absorption cross sections as a function of frequency and identified peaks as corresponding to surface plasmons and single-particle excitations, based on whether the induced charge density (and change in phase thereof) was primarily near the surface or in the interior of the particle. Structure or splitting of the surface plasmon peak was interpreted as coupling between that collective mode and the single particle excitations.

Received: October 25, 2011
Revised: December 1, 2011
Published: December 19, 2011

Prodan, Nordlander, and Halas applied frequency-space TDDFT to jellium nanoshells, examining how their response depends on the inner and outer diameters of the nanoshell,[11] and on the dielectric properties of the materials in the center and outside of the nanoshell.[12] Their results are qualitatively similar to classical and semiclassical calculations and are in good agreement with experiment. Zuloaga, Prodan, and Nordlander, using frequency-space TDDFT to look at dimers of jellium spheres, showed that for very small separations, quantum tunneling and screening significantly reduce electric field enhancements compared to classical models, while at larger separations the classical description is adequate.[13] They also looked at jellium nanorods and saw similar reductions in electric field enhancements due to nonzero electron density outside the particle edges.[14]

More recently, frequency-space TDDFT has been supplemented by real-time TDDFT. Real-time TDDFT differs from frequency-space TDDFT in that it involves an explicit time propagation of the ground-state Kohn−Sham eigenstates with a time-dependent Hamiltonian and yields the electronic density defined at each time step in the propagation. Frequency-space TDDFT calculates a frequency-dependent density from Fourier transformed time-dependent linear-response equations in terms of the ground-state Kohn−Sham eigenstates and the exchange-correlation potential. Both make use of an approximate exchange-correlation potential, typically the adiabatic local density approximation (ALDA), however real-time TDDFT is not explicitly linearized, whereas frequency space computations generally rely on linear versions of the response equations. As a result, real-time TDDFT may be applied in nonlinear regimes, such as strong electric fields.[15]

Yabana and Bertsch,[16] calculating the optical response of atomic clusters, show a near equivalence of frequency-space and real-time methods for a jellium sphere corresponding to the cluster Li_{138}. Real-time TDDFT has been used extensively for investigating the response of jellium or metal clusters to intense laser beams and energetic ion collisions, since linear-response is not obviously an appropriate approximation in these experiments.[17−19]

Yan, Yuan, and Gao have applied real-space real-time TDDFT to linear atomic chains, examining the longitudinal and transverse plasmon resonances, one of which may be unique to the quantum description.[20,21]

We use Octopus, a GNU Public Licensed software package, to do real-space, real-time TDDFT[22,23] on systems of jellium spheres. A ground-state calculation determines the Kohn−Sham eigenstates and their occupation. A finite-temperature smearing of the occupation of the Kohn−Sham eigenstates avoids problems with degeneracies, allowing results for electron numbers corresponding to closed and open electronic shells. We used an electronic temperature of 316 K, which corresponds to an energy one-sixth as large as the spacing between more closely spaced shells. The energy of the main peak in the response spectrum is 175 times this energy.

Once a ground-state solution is calculated, we perform time evolutions using the approximately enforced time-reversal symmetry (AETRS) propagator with a fourth order Taylor expansion of the exponentials. The ground-state Kohn−Sham eigenstates are propagated with a time-dependent Hamiltonian, either one representing a delta function electromagnetic pulse to the system, or a continuous plane-wave of constant frequency. The occupation of the Kohn−Sham levels remains constant, and no new ground state is calculated. The result is an electron density that changes with time in response to the applied potential.

The first propagation we perform determines the response of the system to a linearly polarized delta pulse. The Fourier transform of the dipole moment of the electron density gives the photoabsorption cross section as a function of frequency. This response function shows peaks at the resonant frequencies of the system, as in Figure 1. The width of the peaks is inversely

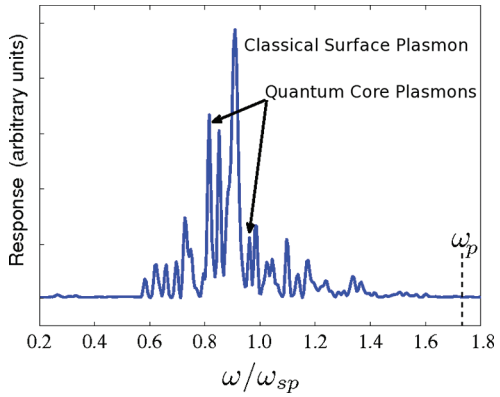

Figure 1. Optical spectrum of a single 100 electron Au-jellium sphere. (r_s = 3 a_0, R = 0.74 nm) The x-axis indicates frequency in units of the classical surface plasmon frequency, ω_{sp}. The bulk plasmon frequency, ω_p, is also indicated.

proportional to the length of the time propagation due to third-order polynomial damping in the Fourier transform of the dipole moment. The area under a peak is the oscillator strength of the transition. Once the resonant frequencies are identified, we characterize the nature of each resonance by examining the response at that frequency. Starting over from the ground state, we drive the system at one of the resonant frequencies by applying an oscillating electromagnetic field. (The applied field does not vary spatially; the size of the MNP is much smaller than the wavelength of light at these frequencies.) To characterize the resonances, we examine the evolution in time, t, of the induced electron density, $\Delta\rho(t) = \rho(t) - \rho_{gs}$, where $\rho(t)$ is the time-dependent electron density and ρ_{gs} is the electron density from the ground state calculation.

We have investigated spherical jellium nanoparticles with 68−600 electrons with a single electron radius of 3 bohr, r_s = 3 a_0, to represent gold. (The sphere radius, R, is 12.2−25.3 a_0 (0.65−1.34 nm) for this range of electron number.)

The spectrum of a 100 electron nanoparticle is shown in Figure 1. The spectrum, consistent with previous similar calculations,[8−10] contains multiple peaks, which could be described as a single peak that is split or fragmented. The largest peak occurs at a frequency of $0.91\omega_{sp}$, where $\omega_{sp} = \omega_p/\sqrt{3} = [(n_e e^2)/(3m\varepsilon_o)]^{1/2}$ is the frequency of a classical surface plasmon (Mie resonance) in a spherical particle with ω_p as the bulk plasma frequency, n_e is the electron density, e and m are the electronic charge and mass, and ε_o is the vacuum permittivity. This calculated surface plasmon energy is close to but red shifted from the classical value ω_{sp}. In the jellium model, there is no screening from core electrons. This absence of screening should blue shift the calculated value. However, the charge density tunnels outside the MNP, which in turn slows the oscillation, that is, causes a red shift from the classical result. This appears to be the dominant effect here. Other significant peaks occur at 0.82, 0.85, 0.98, 0.96, and $0.73\omega_{sp}$.

dx.doi.org/10.1021/nl2037613 | Nano Lett. 2012, 12, 429−434

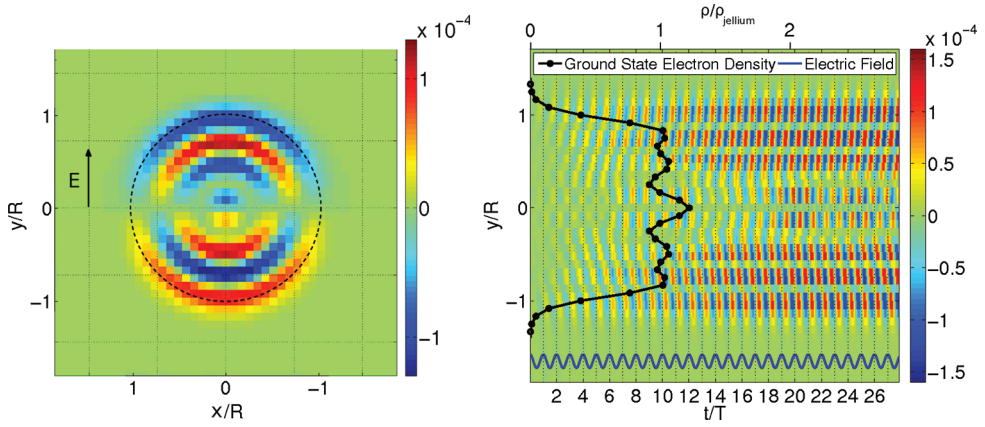

Figure 2. Classical surface plasmon in 100 electron sphere. (a) Induced electron density, $\Delta\rho(x,y)$, after 23.7 periods of the applied field. Cross section through the center of the sphere. The y-axis is parallel to the electric field, which is driving the sphere at an angular frequency of $0.91\omega_{sp}$, the tallest peak from the spectrum in Figure 1. The dashed circle outlines the MNP jellium background. (b) Induced electron density, $\Delta\rho(y,t)$, along the central axis of the sphere. The y-axis is parallel to the electric field, whose strength is indicated in blue near the bottom. The black line indicates the ground-state electron density as a function of position along the y-axis. The density-axis, relevant for that function only, is at the top of the figure.

The "quantum core plasmons" are found among these peaks. In addition to these main peaks, there are features several orders of magnitude smaller. At the frequencies of 0.27 and $0.32\omega_{sp}$ are peaks 2 orders of magnitude smaller than the main peak. Though we have not examined these resonances, they are likely to be single particle transitions, for example, the energy difference between the fully occupied 3s level and the unoccupied 3p level is $0.27\omega_{sp}$. In the frequency range of $2.0-2.2\omega_{sp}$ $(1.2-1.3\omega_p)$, there are four peaks 3 orders of magnitude smaller than the main peak. We identify these with a Landau-damped bulk plasmon,[24] again, without detailed examination of the behavior of the resonances.

To determine the spatial character of the main resonances, we first look at the induced charge density associated with each peak. Figure 2a shows $\Delta\rho(x,y,z = 0, t = 23.7T)$, a cross-section of the induced electron density at a particular instant while the sphere is being driven at its peak resonant frequency, $0.91\omega_{sp}$, where y is position along the central axis parallel to the field, x and z are position along the perpendicular axes, and T is the period of the driving frequency. A full movie showing this cross section of the change in electron density evolving in time is available as Supporting Information.

The spatial character is more fully seen in a plot of the time-dependent induced electron density along the y-axis of the sphere. Figures 2b, 3, and 4 show $\Delta\rho(x = 0, y, z = 0, t)$ as color contours, as a function of y and t for the resonances indicated in Figure 1. To better understand the phase relationship between the oscillations and the applied field, the electric field is plotted along the time axis, and the time-axis ticks are at intervals of the period of the field oscillations. In Figure 2b only, the total ground state electron density is superimposed along the y-axis, indicating the size and position of the nanoparticle.

The MNP being driven at the main peak frequency of $0.91\omega_{sp}$ (Figure 2b) shows a response throughout the particle, and we thus name this resonance a "classical surface plasmon". The response at the frequencies of the other peaks occurs primarily near the center of the particle, and we refer to these resonances as "quantum core plasmons", since they arise only in this quantum treatment of the problem. As can be seen in Figure 2b the magnitude of the response of the particle increases from zero with time, since there is initially no applied field. The build-up is not always monotonic, and its behavior varies for different resonances.

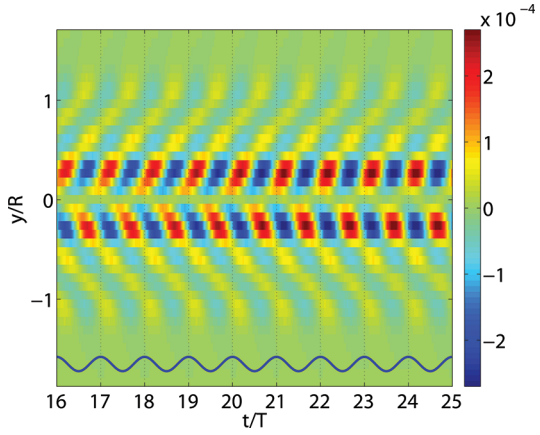

Figure 3. Quantum core plasmon. Closeup of change in electron density $\Delta\rho(y,t)$ when driven at an angular frequency of $0.82\omega_{sp}$.

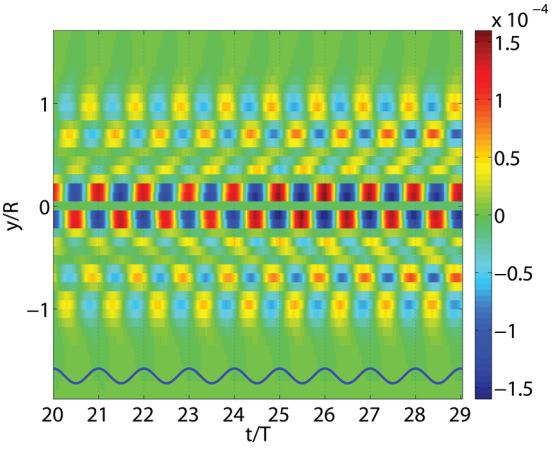

Figure 4. Quantum core plasmon. Closeup of change in electron density $\Delta\rho(y,t)$ when driven at an angular frequency of $0.96\omega_{sp}$.

The classical surface plasmon appears to be made up of surface and core dipole oscillations. That is, there are strong, smaller dipole moments at the outer edges of the particle,

dx.doi.org/10.1021/nl2037613 | Nano Lett. 2012, 12, 429−434

which are in phase with a spatially larger but less intense dipole moment in the core of the particle. The quantum core plasmons are primarily dipole oscillations in the core of the dot (each with slightly different spatial extent) with a less intense surface dipole moment at the edges. The surface dipole may be in or out of phase with the core dipole. In each resonance, the surface oscillation lags the electric field by one-quarter period. The resonance at $0.85\omega_{sp}$ has a mixed character, somewhat similar to the classical surface plasmon at $0.91\omega_{sp}$ and somewhat similar to the quantum core plasmon at $0.82\omega_{sp}$.

Previous authors[8,10,25−27] have interpreted the quantum core plamon resonances as a splitting between the collective surface plasmon and single particle-hole excitations. They have used the distinction between surface and core oscillations to stand-in for a distinction between collective and single-particle oscillations. This may not be justified, as we will discuss next.

The time evolution of the Kohn−Sham states is responsible for the changes in electron densities illustrated in Figures 2b, 3, and 4. To see how a resonance is built up out of these individual single particle states, we project the time-evolved states onto the original ground-state eigenstates, $\langle\phi_n(t)|\phi_m(0)\rangle$.

Figure 5 shows the magnitude-squared of this projection at a time after the MNP has been driven at the surface plasmon

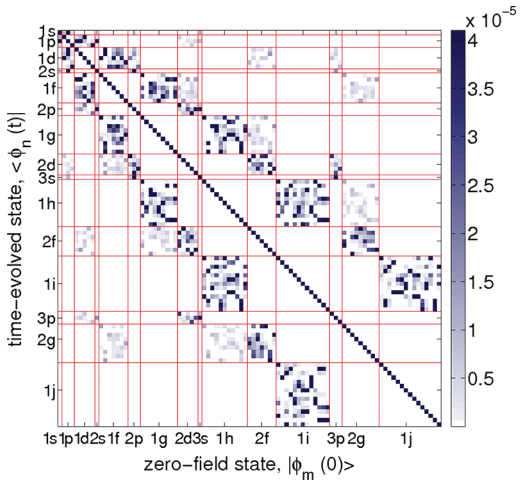

Figure 5. Classical surface plasmon. Magnitude-squared projections, $|\langle\phi_n(t)|\phi_m(0)\rangle|^2$, of the time-evolved Kohn−Sham eigenstates onto the ground state Kohn−Sham eigenstates.

resonant frequency of $0.91\omega_{sp}$ for many periods. The time evolution changes the states only slightly: the magnitude-squared projection of any single-particle ground state with its own time-evolved state, $|\langle\phi_n(t)|\phi_n(0)\rangle|^2$, seen along the diagonal, is at most only five parts in a thousand different from one. The grouping inside the red lines indicates shell structure. As can be seen, the transitions that do occur are between states $\phi_n(t)$ and $\phi_m(0)$ whose angular momentum differs by 1. Finally, Figure 5 shows that many transitions are involved in the classical surface plasmon resonance, rather than the response being dominated by a single electron transition. This is the case for all of the resonances we have examined here. Each of these plots of projections looks similar to Figure 5. This implies that there is no significant single-particle transition occurring in any of the resonances we have examined. The transitions that make up the collective response are similar in strength. If the splitting of the response peak were the result of the interaction of the plasmon resonance with single-particle transitions, one would expect those single-particle transitions to be visible in this plot of the projections, and to be significantly larger than the transitions making up the collective plasmon resonance. An example of a single-particle transition in a MNP far from the plasmon frequency is shown in the work of Quijada et al.[28] That work shows a single projection growing in time as the system is driven at a single frequency.

Figure 5 shows all the states included in our ground-state and time-dependent calculations, although many of them do not contribute significantly to the charge density. The Fermi level is in the 2f shell, each state of which is occupied by 1.13 electrons. Lower energy states are all doubly occupied, and the 1i state is already very sparsely occupied by 0.0065 electrons.

To better understand how each state contributes to the spatial character of a particular resonance we look at the magnitude-squared of each time-dependent Kohn−Sham wave function, multiplied by its occupation, $\rho_n(y,t) = N(n)|\langle\phi_n(y,t)|\phi_n(y,t)\rangle|^2$, where $N(n)$ is the occupation of level n. Figure 6

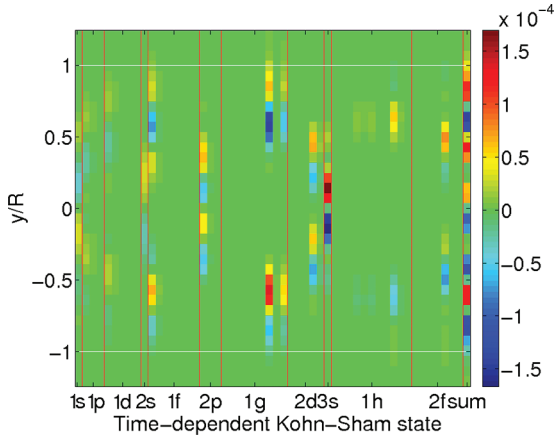

Figure 6. Contribution to change in electron density due to each time-evolved Kohn−Sham eigenstate. Classical surface plasmon ($0.91\omega_{sp}$). The last column shows the sum over all eigenstates.

shows the position-dependence of each Kohn−Sham state's contribution to the change in electron density for the main plasmon resonance at a single time. The position along the central axis of the dot is on the y-axis, while the energy eigenstates of the system are along the x-axis. Vertical red lines separate the energy eigenstate shells, horizontal white lines mark the edges of the jellium sphere. The sum over all states, which is equal to the total change in electron density, is appended to the right edge of the plot. Because the states above the 2f-shell have very low occupations, they do not contribute significantly to the electron density and are omitted from the figures. Figure 7 shows a similar plot for one of the quantum core plasmons.

Figure 6 and Figure 7 show that both resonances involve multiple states that add constructively or deconstructively to create the charge oscillations seen either throughout the dot or confined to the core. Similar states participate in each oscillation, for example, $l = 0$ s-states become polarized because electrons in these states can only make transitions to $l = 1$ states. Each state that is involved in the quantum core plasmon is involved in the surface plasmon but not vice versa. The surface plasmon has significant contribution to the charge oscillation from 1f and 1g states that are the principal contribution closest to the surface of the dot. These

dx.doi.org/10.1021/nl2037613 | Nano Lett. 2012, 12, 429−434

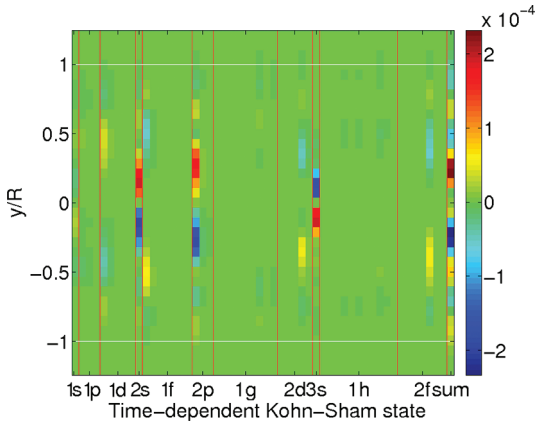

Figure 7. Contribution to change in electron density due to each time-evolved Kohn–Sham eigenstate. Quantum core plasmon ($0.82\omega_{sp}$). The last column shows the sum over all eigenstates.

observations do not suggest that the quantum core plasmon results from a splitting between the collective oscillation and a single particle oscillation.

This work is focused on the quantum limit of very small MNPs that still have enough electrons to sustain a plasmon resonance. So far most of our work has been with 100 electron MNPs, which are a good size for this purpose. However we have examined MNPs with as many as 600 electrons. Figure 8

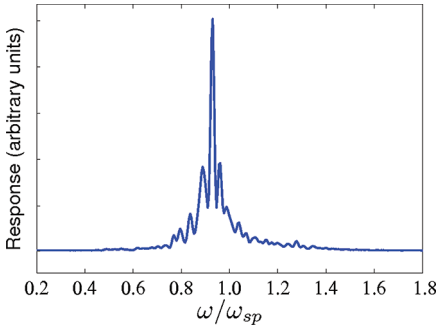

Figure 8. Optical spectrum of a single 600 electron Au-jellium sphere. (r_s = 3 a_0, R = 1.34 nm).

shows the response of the 600 electron MNP to a delta pulse. The 600 electron MNP has a strong main resonance and secondary resonances at frequencies similar to the resonances described here for the 100 electron dot. (The classical surface plasmon frequency, ω_{sp}, is not dependent on the size of the particle.) However in the 600 electron MNP the primary resonance is more than twice as strong as the secondary resonances. It is reasonable to expect the quantum core plasmon resonances to be significantly less important as we move to larger particle sizes. As seen in Figure 9, the primary resonance in the 600 electron MNP also appears throughout the whole particle, but the strongest response is at the surface of the particle, which is also expected in a transition to more classical behavior.

The presence of quantum core plasmons may have implications for the field of nanoplasmonics in systems where MNPs lie very near to optical emitters. For very short distance scales, there may be less nonradiative transfer of energy from the emitter into core plasmons because the core oscillations are deeper in the particle. We plan to examine such multiple-

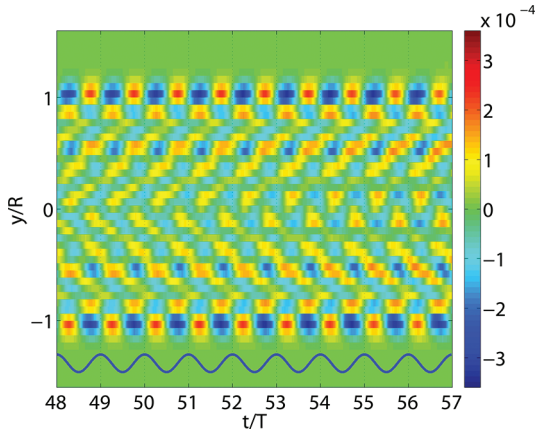

Figure 9. Classical surface plasmon in 600 electron MNP. Closeup of change in electron density $\Delta\rho(y,t)$ when driven at main plasmon resonance.

element systems with a unified quantum approach in future work. We speculate that for small particles, the number of core plasmons should increase with increasing number of electrons. For large particles, the number of strong core plasmons decreases as the plasmonic excitations become localized to the surface.

Metallic nanoparticles in the quantum regime exhibit multiple resonances that correspond to plasmon resonances. They all exhibit collective behavior, being composed of multiple transitions which follow the selection rule $\Delta l = \pm 1$. The resonances are most distinguished by the region of the nanoparticle in which the charge oscillates. Quantum core plasmons exist as a charge oscillation that occurs primarily near the center of the particle with a less intense surface oscillation that may be in or out of phase with the core oscillations. The resonance most analogous to the classical surface plasmon exhibits charge oscillation throughout the particle. As the particle size increases, the classical surface plasmon dominates the quantum core plasmon and becomes more concentrated near the surface of the particle.

■ ASSOCIATED CONTENT

Ⓢ Supporting Information

The file 133131DensitySmall.mpg is a movie showing how the change in electron density evolves in time in the classical surface plasmon. This material is available free of charge via the Internet at http://pubs.acs.org.

■ AUTHOR INFORMATION

Corresponding Author

*E-mail: (E.T.) ETownsend@eml.cc; (G.W.B.) Garnett.Bryant@nist.gov.

■ REFERENCES

(1) Artuso, R. D.; Bryant, G. W. *Nano Lett.* **2008**, *8*, 2106–2111, PMID: 18558787

(2) Artuso, R. D.; Bryant, G. W. *Phys. Rev. B* **2010**, *82*, 195419.

(3) Artuso, R. D.; Bryant, G. W.; Garcia-Etxarri, A.; Aizpurua, J. *Phys. Rev. B* **2011**, *83*, 235406.

(4) Manjavacas, A.; Garciá de Abajo, F. J.; Nordlander, P. *Nano Lett.* **2011**, *11*, 2318–2323.

(5) Ridolfo, A.; Di Stefano, O.; Fina, N.; Saija, R.; Savasta, S. *Phys. Rev. Lett.* **2010**, *105*, 263601.

(6) Waks, E.; Sridharan, D. *Phys. Rev. A* **2010**, *82*, 043845.

(7) Crowell, J.; Ritchie, R. H. *Phys. Rev.* **1968**, *172*, 436−440.
(8) Ekardt, W. *Phys. Rev. B* **1985**, *31*, 6360−6370.
(9) Puska, M. J.; Nieminen, R. M.; Manninen, M. *Phys. Rev. B* **1985**, *31*, 3486−3495.
(10) Beck, D. E. *Phys. Rev. B* **1987**, *35*, 7325−7333.
(11) Prodan, E.; Nordlander, P. *Nano Lett.* **2003**, *3*, 543−547.
(12) Prodan, E.; Nordlander, P.; Halas, N. J. *Chem. Phys. Lett.* **2003**, *368*, 94−101.
(13) Zuloaga, J.; Prodan, E.; Nordlander, P. *Nano Lett.* **2009**, *9*, 887−891, PMID: 19159319
(14) Zuloaga, J.; Prodan, E.; Nordlander, P. *ACS Nano* **2010**, *4*, 5269−5276.
(15) Castro, A.; Marques, M. A.; Alonso, J. A.; Rubio, A. *J. Comput. Theor. Nanosci.* October **2004**, *1*, 231−255(25)
(16) Yabana, K.; Bertsch, G. F. *Phys. Rev. B* **1996**, *54*, 4484−4487.
(17) Calvayrac, F.; Reinhard, P. G.; Suraud, E. *Phys. Rev. B* **1995**, *52*, R17056−R17059.
(18) Calvayrac, F.; Reinhard, P. G.; Suraud, E. *Ann. Phys.* **1997**, *255*, 125−162.
(19) Calvayrac, F.; Reinhard, P. G.; Suraud, E.; Ullrich, C. A. *Phys. Rep.* **2000**, *337*, 493−578.
(20) Yan, J.; Yuan, Z.; Gao, S. *Phys. Rev. Lett.* **2007**, *98*, 216602.
(21) Yan, J.; Gao, S. *Phys. Rev. B* **2008**, *78*, 235413.
(22) Marques, M. A. L.; Castro, A.; Bertsch, G. F.; Rubio, A. *Comput. Phys. Commun.* **2003**, *151*, 60−78.
(23) Castro, A.; Appel, H.; Oliveira, M.; Rozzi, C. A.; Andrade, X.; Lorenzen, F.; Marques, M.; Gross, E.; Rubio, A. *Phys. Status Solidi B* **2006**, *243*, 2465−2488.
(24) Bohm, D.; Gross, E. P. *Phys. Rev.* **1949**, *75*, 1851−1864.
(25) Yannouleas, C.; Broglia, R. A.; Brack, M.; Bortignon, P. F. *Phys. Rev. Lett.* **1989**, *63*, 255−258.
(26) Yannouleas, C.; Broglia, R. A. *Phys. Rev. A* **1991**, *44*, 5793−5802.
(27) Brack, M. *Rev. Mod. Phys.* **1993**, *65*, 677−732.
(28) Quijada, M.; Muiño, R. D.; Borisov, A. G.; Alonso, J. A.; Echenique, P. M. *New J. Phys.* **2010**, *12*, 053023.